*Inorg. Chem.* **2008**, *47*, 11501−11513

# Synthesis, Structures, and Luminescence Properties of Lanthanide Complexes with Structurally Related New Tetrapodal Ligands Featuring Salicylamide Pendant Arms

**Xueqin Song,[†] Xiaoyan Zhou,[‡] Weisheng Liu,*[,‡] Wei Dou,[‡] Jingxin Ma,[‡] Xiaoliang Tang,[‡] and Jiangrong Zheng[‡]**

*College of Chemistry and Chemical Engineering and State Key Laboratory of Applied Organic Chemistry, Lanzhou University, Lanzhou 730000, China, and School of Chemical and Biological Engineering, Lanzhou Jiaotong University, Lanzhou 730070, China*

Received May 6, 2008

To explore the relationships between the structures of ligands and their complexes, we have synthesized and characterized a series of lanthanide complexes with two structurally related ligands, 1,1,1,1-tetrakis{[(2′-(2-benzylaminoformyl))phenoxyl]methyl}methane ($L^{I}$) and 1,1,1,1-tetrakis{[(2′-(2-picolyaminoformyl))phenoxyl]methyl}methane ($L^{II}$). A series of zero- to three-dimensional lanthanide coordination complexes have been obtained by changing the substituents on the Pentaerythritol. Our results revealed that, complexes of the $L^{I}$ ligand, $\{Ln_4L^{I}_3(NO_3)_{12}\cdot nC_4H_{10}O\}_\infty$ (Ln = Nd, Eu, Tb, Er, $n = 3$ or 6)] show the binodal 3,4-connected three-dimensional interpenetration coordination polymers with topology of a $(8^3)_4(8^6)_3$ notation. Compared to $L^{I}$, complexes of $L^{II}$ present a cage-like homodinuclear $[Ln_2L^{II}_2(NO_3)_6\cdot 2H_2O]\cdot nH_2O$ (Ln = Nd, Tb, Dy, $n = 0$ or 1) or a helical one-dimensional coordination $\{[ErL^{II}(NO_3)_3\cdot H_2O]\cdot H_2O\}_\infty$ polymer. The luminescence properties of the resulting complexes formed with ions used in fluoroimmunoassays (Ln = Eu, Tb) are also studied in detail. It is noteworthy that subtle variation of the terminal group from benzene to pyridine not only sensibly affects the overall molecular structures but also the luminescence properties as well.

## Introduction

Coordination polymers are presently playing a prominent role in material science,[1] and their potential as functional materials is clearly recognized. The construction of supramolecular networks containing lanthanide ions as connectors is particularly attractive because of the magnetic and electronic properties of 4f ions, which should result in the application of lanthanide polymers in sensors, lighting devices, and optical storage.[2] In contrast to the fruitful production of metal-organic frameworks (MOFs) with d-block transition metal ions, the design and control over high-dimensional lanthanide-based frameworks is currently a formidable task owing to their high and variable coordination numbers and flexible coordination environments.[3,4] On the other hand, lanthanide ions, with their high coordination flexibility and their lack of preferential geometries, are good candidates to provide unique opportunities for the discovery of unusual network topologies,[5−7] thus leading us to this

* To whom correspondence should be addressed. E-mail: liuws@lzu.edu.cn. Phone: +86-931-8915151. Fax: +86-931-8912582.
† Lanzhou Jiaotong University.
‡ Lanzhou University.

(1) Kitagawa, S.; Noro, S. *Comprehensive Coordination Chemistry II*; Elsevier Ltd.: Oxford, U.K., 2004; Vol. *3*; Janiak, C. *Dalton Trans.*, **2003**, 2781.

(2) (a) Kuriki, K.; Koike, Y.; Okamoto, Y. *Chem. Rev.* **2002**, *102*, 2347. (b) Cahill, C. L.; de Lill, D. T.; Frisch, M. *CrystEngComm* **2007**, *9*, 15. (c) Gschneidner, K. A., Jr.; Pecharsky, V., Bünzli, J.-C. G., Guillou, O.; Daiguebonne, C., *Handbook on the Physics and Chemistry of Rare Earths*; Elsevier: Amsterdam, The Netherlands, 2005; Vol. *34*; (d) Hill, R. J.; Long, D. L.; Hubberstey, P.; Schröder, M.; Champness, N. R. *J. Solid State Chem.* **2005**, *178*, 2414. (e) Bünzli, J. C. G.; Piguet, C. *Chem. Soc. Rev.* **2005**, *34*, 1048. (f) Robin, A. Y.; Fromm, K. M. *Coord. Chem. Rev.* **2006**, *250*, 2127. (g) Faulkner, S.; Matthews, J. L. *Comprehensive Coordination Chemistry II*; Elsevier: Oxford, U.K., 2004; Vol. *9*, p 913. (h) Piguet, C.; Bünzli, J.-C. G. *Chem. Soc. Rev.* **1999**, *28*, 347. (i) Gheorghe, R.; Cucos, P.; Andruh, M.; Costes, J. P.; Donnadieu, B.; Shova, S. *Chem.—Eur. J.* **2005**, *12*, 187.

(3) Kiritsis, V.; Michaelides, A.; Skoulika, S.; Golhen, S.; Ouahab, L. *Inorg. Chem.* **1998**, *37*, 3407.

(4) (a) Reineke, T. M.; Eddaoudi, M.; Moler, D.; O'Keeffe, M.; Yaghi, O. M. *J. Am. Chem. Soc.* **2000**, *122*, 4843. (b) Pan, L.; Adams, K. M.; Hernandez, H. E.; Wang, X. T.; Zheng, C.; Hattori, Y.; Kaneko, K. *J. Am. Chem. Soc.* **2003**, *125*, 3062. (c) Zhao, B.; Cheng, P.; Chen, X. Y.; Cheng, C.; Shi, W.; Liao, D. Z.; Yan, S. P.; Jiang, Z. H. *J. Am. Chem. Soc.* **2004**, *126*, 3012.

10.1021/ic8008267 CCC: $40.75 
Published on Web 11/08/2008

**Scheme 1.** Schematic Illustration of Ligands $L^I$ and $L^{II}$

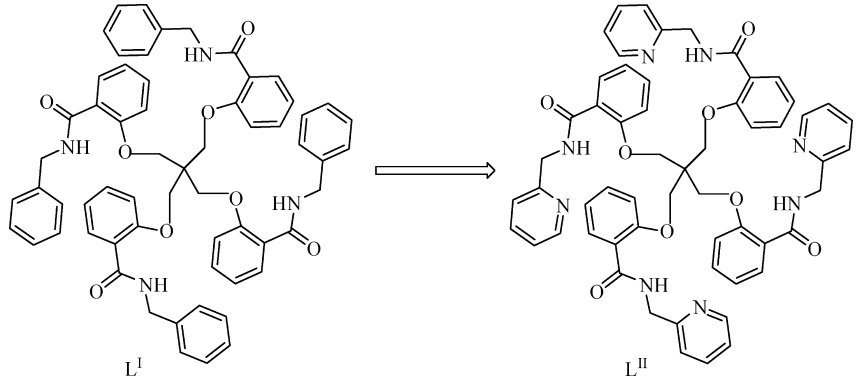

interesting and challenging field. So far, much work is focused on using multicarboxylate ligands to prepare lanthanide-containing MOFs.[8] By contrast, based on a query to the Cambridge Structural Database (CSD), we find that the synthesis of multidimensional lanthanide-containing MOFs by using amide ligands is less developed.[9]

In many cases it is quite difficult to design and synthesize a desired MOF in a truly deliberate manner because of the influence of many factors upon the final product structures, such as the coordination geometry of the central metal ion and the shape, functionality, flexibility, and symmetry of the ligand.[10] Presently, a rational synthetic strategy widely used in this area is the linking of metal ions with polydentate ligands that function as connectors.[11] Polydentate ligand compounds, which provide metal-binding sites, can act as either bridging or chelating ligands, yielding desired networks in metal-organic coordination polymers.[12] To better control the geometry and properties of the final lanthanide framework, we have chosen to use a new topological approach[13] in which suitable building blocks are implemented[14] into a multidentate linker with a flexible spacer, which directs the geometry and dimensionality of the self-assembled network. Salicylamide derived ligands are efficient sensitizers of lanthanide luminescence.[15] We are interested in how different terminal groups of salicylamide ligands impact the structures of various lanthanide metal complexes, as well as the luminescence properties. Replacement of the benzene unit of the salicylamide group by a pyridine ring introduces a nitrogen center that may serve as a further supramolecular interaction site and markedly modify the coordination properties of the ligand. On account of the large steric factor and poor flexibility of the ligands, the high coordination numbers of lanthanide may be satisfied with nitrate anion possessing strong coordination abilities. Thus, as a part of our systemic investigation of lanthanide coordination polymers based on the ligands of this type, we chose the following tetrapodal ligands (Scheme 1) and lanthanide nitrate in our experiments to investigate the influence of terminal groups and cations.

As a result, a series of novel coordination complexes with a variety of zero-, one-, and three-dimensional frameworks were isolated. These compounds, namely, $\{[Pr_4L^I_3(NO_3)_{12}\cdot 3C_4H_{10}O\}_\infty$ (**1**), $\{[Eu_4L^I_3(NO_3)_{12}\cdot 6C_4H_{10}O\}_\infty$ (**2**), $\{[Tb_4L^I_3(NO_3)_{12}\cdot 6C_4H_{10}O\}_\infty$ (**3**), $\{[Er_4L^I_3(NO_3)_{12}\cdot 3C_4H_{10}O\}_\infty$ (**4**) ($L^I$ = 1,1,1,1-tetrakis{[(2′-(2-benzylaminoformyl))phenoxyl]methyl}methane), and $Nd_2L^{II}_2(NO_3)_6(H_2O)_2$ (**5**), $[Tb_2L^{II}_2(NO_3)_6(H_2O)_2\cdot H_2O$ (**6**) and $Dy_2L^{II}_2(NO_3)_6(H_2O)_2\cdot H_2O$ (**7**) $\{[ErL^{II}(NO_3)_3(H_2O)]\cdot H_2O\}_\infty$ (**8**) ($L^{II}$ = 1,1,1,1-tetrakis{[(2′-(2-picolyaminoformyl))phenoxyl]methyl}methane), were synthesized by the solution evaporation method and characterized via single-crystal X-ray diffraction analysis, IR, elemental analysis. The luminescence properties of the resulting complexes formed with ions


(5) (a) Liu, W. S.; Jiao, T. Q.; Li, Y. Z.; Liu, Q. Z.; Tan, M. Y.; Wang, H.; Wang, L. F. *J. Am. Chem. Soc.* **2004**, *126*, 2280. (b) Ma, B. Q.; Zhang, D. S.; Gao, S.; Jin, T. Z.; Yan, C. H.; Xu, G. X. *Angew. Chem., Int. Ed.* **2000**, *39*, 3644. (c) Serre, C.; Stock, N.; Bein, T.; Férey, G. *Inorg. Chem.* **2004**, *43*, 3159.

(6) (a) Mancino, G.; Ferguson, A. J.; Beeby, A.; Long, N. J.; Jones, T. S. *J. Am. Chem. Soc.* **2005**, *127*, 524. (b) Reineke, T. M.; Eddaoudi, M.; Fehr, M.; Kelley, D.; Yaghi, O. M. *J. Am. Chem. Soc.* **1999**, *121*, 1651. (c) Guo, X.; Zhu, G.; Fang, Q.; Xue, M.; Tian, G.; Sun, J.; Li, X.; Qiu, S. *Inorg. Chem.* **2005**, *44*, 3850.

(7) (a) Luo, F.; Che, Y. X.; Zheng, J. M. *Cryst. Growth Des.* **2006**, *6*, 2432. (b) Hu, D. X; Luo, F.; Che, Y. X.; Zheng, J. M. *Cryst. Growth Des.* **2007**, *7*, 1733.

(8) (a) Pan, L.; Li, X. J.; Wu, Y.; Zheng, N. *Angew. Chem., Int. Ed.* **2000**, *39*, 527. (b) Reineke, T. M.; Eddaoudi, M.; O'Keeffe, M.; Yaghi, O. M. *Angew. Chem., Int. Ed.* **1999**, *38*, 2590. (c) Pan, L.; Adams, M. K.; Hernandez, H. E.; Wang, X. T.; Zheng, C.; Hattori, Y.; Kaneko, K. *J. Am. Chem. Soc.* **2003**, *125*, 3062. (d) Reineke, T. M.; Eddaoudi, M.; Moler, D.; O'Keeffe, M.; Yaghi, O. M. *J. Am. Chem. Soc.* **2000**, *122*, 4843. (e) Guo, X. D.; Zhu, G. S.; Fang, Q. R.; Xue, M.; Tian, G.; Sun, J. Y.; Li, X. T.; Qiu, S. L. *Inorg. Chem.* **2006**, *44*, 3850. (f) Daiguebonne, C.; Kerbellec, N.; Bernot, K.; Gérault, Y.; Deluzet, A.; Guillou, O. *Inorg. Chem.* **2006**, *45*, 5399. (g) Qin, C.; Wang, X.-L.; Wang, E.-B.; Su, Z.-M. *Inorg. Chem.* **2005**, *44*, 7122. (h) Zhang, Z.-H.; Okamura, T.; Hasegawa, Y.; Kawaguchi, H.; Kong, L.-Y.; Sun, W.-Y.; Ueyama, N. *Inorg. Chem.* **2005**, *44*, 6219. (i) Marchal, C.; Filinchuk, Y.; Imbert, D.; Bünzli, J.-C. G.; Mazzanti, M. *Inorg. Chem.* **2007**, *46*, 6242.

(9) Sun, R.; Wang, S. N.; Xing, H.; Bai, J. F.; Li, Y. Z.; Pan, Y.; You, X. Z. *Inorg. Chem.* **2007**, *46*, 8451.

(10) Sun, D. F.; Cao, R.; Sun, Y. Q.; Bi, W. H.; Yuan, D. Q.; Shi, Q.; Li, X. *Chem. Commun.* **2003**, 1528.

(11) Chu, D. Q.; Xu, J. Q.; Duan, L. M.; Wang, T. G.; Tang, A. Q.; Ye, L. *Eur. J. Inorg. Chem.* **2001**, 1135.

(12) (a) Yong, G. P.; Wang, Z. Y.; Cui, Y. *Eur. J. Inorg. Chem.* **2004**, 4317. (b) Cao, R.; Sun, D. F.; Liang, Y. C.; Hong, M. C.; Tatsumi, K.; Shi, Q. *Inorg. Chem.* **2002**, *41*, 2087. (c) Zaworotko, M. J. *Angew.Chem., Int. Ed.* **1998**, *37*, 1211. (d) Chang, F.; Wang, Z. M.; Sun, H. L.; Wen, G. H.; Zhang, X. X. *Dalton Trans.* **2005**, 2976.

(13) Rowan, S. J.; Hamilton, D. G.; Brady, P. A.; Sanders, J. K. M. *J. Am. Chem. Soc.* **1997**, *119*, 2578.

(14) Hosseini, M. W. *Chem. Commun.* **2005**, 5825.

**Table 1.** Elemental Analytical and IR Spectral Data for the Complexes

| compound | elemental analyses[a] C | H | N | Ln | IR($\lambda_{max}$/cm$^{-1}$) $\nu$(C=O) | |
|---|---|---|---|---|---|---|
| $Pr_4(NO_3)_{12}\cdot L^I_3\cdot 3C_4H_{10}O$ | 52.76 (52.64) | 4.47 (4.49) | 7.59 (7.56) | 12.70 (12.67) | 1604 | |
| $Eu_4(NO_3)_{12}\cdot L^I_3\cdot 6C_4H_{10}O$ | 52.48 (52.72) | 4.85 (4.87) | 7.10 (7.13) | 12.83 (12.89) | 1603 | |
| $Tb_4(NO_3)_{12}\cdot L^I_3\cdot 6C_4H_{10}O$ | 52.29 (52.41) | 4.80 (4.82) | 7.06 (7.09) | 13.37 (13.40) | 1604 | |
| $Er_4(NO_3)_{12}\cdot L^I_3\cdot 3C_4H_{10}O$ | 51.36 (51.42) | 4.41 (4.38) | 7.34 (7.38) | 14.62 (14.69) | 1602 | |
| $Nd(NO_3)_3\cdot L^{II}\cdot H_2O$ | 51.52 (51.66) | 4.13 (4.11) | 11.66 (11.63) | 10.93 (10.88) | 1603 | 1635 |
| $Tb(NO_3)_3\cdot L^{II}\cdot 3/2H_2O$ | 50.60 (50.75) | 4.12 (4.11) | 11.37 (11.42) | 11.72 (11.78) | 1604 | 1638 |
| $Dy(NO_3)_3\cdot L^{II}\cdot 3/2H_2O$ | 50.49 (50.61) | 4.07 (4.10) | 11.35 (11.39) | 11.96 (12.01) | 1604 | 1632 |
| $Er(NO_3)_3\cdot L^{II}\cdot 2H_2O$ | 50.01 (50.10) | 4.11 (4.13) | 11.22 (11.28) | 12.19 (12.24) | 1605 | 1638 |

[a] Data in parentheses are calculated values.

used in fluoroimmunoassays (Ln = Eu, Tb) are also studied in detail.

## Experimental Section

**Synthesis of Ligand.** The ligand 1,1,1,1-tetrakis{[(2′-(2-benzylaminoformyl))phenoxyl]methyl}methane ($L^I$), and 1,1,1,1-tetrakis{[(2′-(2-picolyaminoformyl))phenoxyl]methyl}methane ($L^{II}$) were prepared by the following synthetic routes. To a solution of Pentaerythritol benzenesulfonate[16] (2.32 g, 3.3 mmol) in dry dimethylformamide (DMF) was added $K_2CO_3$ (0.69 g, 5 mmol) and the mixture stirred and heated for 10 min. Salicylamide[17] (15 mmol) in 50 mL of DMF was added dropwise in 30 min, and the resulting solution stirred and heated to reflux for 12 h. After cooling down, inorganic salts were separated by filtration, and the solvent removed from the filtrate under reduced pressure. The crude product was purified by chromatography on silica, gradient elution from petroleum to 10:1 petroleum-ethyl acetate for $L^I$ and 5:1 petroleum-ethyl acetate for $L^{II}$. $L^I$: 2.79 g, Yield, 87%. m.p.: 169.1 °C. Analytical data, Calcd for $C_{61}H_{56}N_4O_8$: C, 75.29; H, 5.61; N, 5.20; Found: C, 75.59; H, 5.59; N, 5.18. IR (KBr, $\nu$, cm$^{-1}$): 3418 (m, NH), 1650 (s, C=O), 1600 (m), 1522 (s), 1486 (m), 1452 (m), 1293 (m), 1221 (s), 755 (s), 670 (s). $^1$H NMR ($CDCl_3$, 300 MHz): $\delta$: $^1$H NMR ($CDCl_3$, 300 MHz): $\delta$: 4.16 (d, $J$ = 5.6, 8H, $NHCH_2$), 4.62 (s, 8H, $OCH_2$), 7.01 (d, $J$ = 8.4, 4H, Ar), 7.32−7.45 (m, 24H, Ar), 7.68 (t, $J$ = 7.2, 4H, Ar), 7.89 (dd, $J$ = 7.8, 4H, Ar), 8.37(s, 4H, NH). ESI-MS: $m/z$ 973.2 [$L^IH^+$].

$L^{II}$: 1.55 g, Yield, 48%. m.p.: 158.7 °C. Analytical data, Calcd for $C_{57}H_{52}N_8O_8$: C, 70.07; H, 5.36; N, 11.47; Found: C, 70.24; H, 5.37; N, 11.42. IR (KBr, $\nu$, cm$^{-1}$): 3401 (m, NH), 1638 (s, C=O), 1598 (m), 1512 (m), 1483 (m), 1220 (s), 1012 (m), 755 (s). $^1$H NMR ($CDCl_3$, 300 MHz): $\delta$: 4.71 (d, $J$ = 4.5, 8H, $NHCH_2$), 4.79 (s, 8H, $OCH_2$), 6.85 (d, $J$ = 8.4, 4H, Ar), 7.00 (t, $J$ = 7.3, 8H, Ar), 7.19−7.29 (m, 16H, Ar), 7.54 (s, 4H, Ar), 8.03 (d, $J$ = 7.8, 4H, Ar), 8.27 (d, $J$ = 4.5, 4H, Ar), 8.37(s, 4H, NH). ESI-MS: $m/z$ 977.2 [$L^{II}H^+$].

**Synthesis of Lanthanide Nitrate Complex.** One millimole of ligand and 1 equiv (1 mmol) of the lanthanide nitrates were dissolved in a hot methanol + ethyl acetate (v/v = 1:10) solution to make a concentrated solution. Then the flask was cooled, and the mixture was filtered into a sealed 25−40 mL glass vial for crystallization at room temperature. After about three weeks crystals suitable for analysis were obtained. IR and elemental analysis data for all complexes are summarized in Table 1.

**Materials and Instrumentation.** The commercially available chemicals were used without further purification. All of the solvents used were of analytical reagent grade.

The metal ions were determined by ethylenediaminetetraacetic acid (EDTA) titration using xylenol orange as indicator. C, N, and H were determined using an Elementar Vario EL. Melting points were determined on a Kofler apparatus. IR spectra were recorded on Nicolet FT-170SX instrument using KBr discs in the 400−4000 cm$^{-1}$ region. Electronic spectra were recorded with a Varian Cary 100 spectrophotometer in acetonitrile solution. $^1$H NMR spectra were measured on a Brucker DRX 300 spectrometer in $CDCl_3$ solution with TMS as internal standard. Fluorescence measurements were made on FLS920 of Edinburgh Instrument equipped with quartz curets of 1 cm path length with a xenon lamp as the excitation source. An excitation and emission slit of 1 or 2.5 nm were used for the measurements of luminescence in solid state. The 77 K solution-state phosphorescence spectra were recorded with solution samples loaded in a quartz tube inside a quartz-walled optical Dewar flask filled with liquid nitrogen in the phosphorescence mode. Quantum yields were determined by an absolute method using an integrating sphere on FLS920 of Edinburgh Instrument. The luminescence decays were recorded using a pumped dye laser (Lambda Physics model FL2002) as the excitation source. The nominal pulse width and the line width of the dye-laser output were 10 ns and 0.18 cm$^{-1}$, respectively. The emission of a sample was collected by two lenses into a monochromator (WDG30), detected by a photomultiplier and processed by a Boxcar Average (EGG model 162) in line with a microcomputer. Reported luminescence lifetimes are averages of at least three independent determinations.

**X-ray Diffraction Studies.** Single-crystal X-ray diffraction measurements were carried out on a Bruker SMART 1000 CCD diffractometer operating at 50 KV and 30 mA using Mo Kα radiation ($\lambda$ = 0.71073 Å). Each selected crystal was mounted inside a Lindemann glass capillary for data collection using the SMART and SAINT software. An empirical absorption correction was applied using the SADABS program. All the structures were solved by direct methods and refined by full-matrix least-squares on $F^2$ using the SHELXTL-97 program package.[18] All non-hydrogen atoms were subjected to aniostropic refinement, and all hydrogen atoms except those of lattice water molecules and disordered carbon atoms of complex **8** which could not be located were added in idealized positions and refined isotropically. Hydrogen atoms of aqua ligands in complexes **5**−**8** and hydrogen atoms of the lattice water molecules in complexes **6** and **7** were located from difference electronic Fourier maps. Crystal data and details of the refinement for 1−8 are summarized in Tables 2 and 3, representative bond lengths (Å) and angles (deg) are presented in Supporting Information, Tables S1−S8, respectively.

(15) (a) Zhang, J.; Tang, Y.; Tang, N.; Tan, M.-Y.; Liu, W.-S.; Yu, K.-B. *J. Chem. Soc., Dalton. Trans.* **2002**, 832. (b) Tang, Y.; Zhang, J.; Liu, W.-S.; Tan, M.-Y.; Yu, K.-B. *Polyhedron* **2005**, *24*, 1160. (c) Song, X.-Q.; Dou, W.; Liu, W.-S.; Guo, Y.-L.; Tang, X.-L. *Inorg. Chem. Commun.* **2007**, *10*, 1058. (d) Song, X.-Q.; Liu, W.- S.; Dou, W.; Wang, Y.-W.; Zheng, J.-R.; Zang, Z.-P. *Eur. J. Inorg. Chem.* **2008**, 1901.

(16) Farber, S.; Conley, R. T. *Synth. Commun.* **1974**, *4* (4), 243.

(17) Jiri, Z.; Magdalena, P.; Petr, H.; Milos, T. *Synthesis* **1994**, *110*, 1132.

**Table 2.** Crystal Data and Structure Refinement Parameters for Coordination Polymers **1**−**4**

| | **1** | **2** | **3** | **4** |
|---|---|---|---|---|
| empirical formula | $C_{195}H_{198}N_{24}O_{63}Pr_4$ | $C_{207}H_{228}Eu_4N_{24}O_{66}$ | $C_{207}H_{228}N_{24}O_{66}Tb_4$ | $C_{195}H_{198}Er_4N_{24}O_{63}$ |
| $M_r$ | 4449.41 | 14148.01 | 14231.53 | 4554.81 |
| crystal system | rhombohedral | rhombohedral | rhombohedral | rhombohedral |
| space group | *R*3*c* | *R*3*c* | *R*3*c* | *R*3*c* |
| *a*/Å | 39.597(2) | 39.604(9) | 39.560(2) | 39.386(2) |
| *b*/Å | 39.597(2) | 39.604(9) | 39.560(2) | 39.386(2) |
| *c*/Å | 24.266(3) | 24.300(15) | 24.2198(14) | 24.133(3) |
| $\gamma$/deg | 120 | 120 | 120 | 120 |
| *V*/Å | 32949(4) | 33008(23) | 32826(3) | 32421(5) |
| *Z* | 6 | 6 | 6 | 6 |
| $D_c$ /kg m$^{-3}$ | 1.345 | 1.423 | 1.440 | 1.400 |
| $\mu$/mm$^{-1}$ | 0.956 | 1.213 | 1.366 | 1.623 |
| *F*(000) | 13656 | 14508 | 14556 | 13872 |
| crystal size/mm | 0.16 × 0.14 × 0.10 | 0.63 × 0.55 × 0.49 | 0.45 × 0.36 × 0.24 | 0.36 × 0.33 × 0.28 |
| $\theta$ range for data collection/deg | 2.72−25.01 | 1.78−25.01 | 1.78−25.00 | 1.79−25.01 |
| index ranges, *hkl* | $-47 \le h \le <45$ | $-47 \le h \le 46$ | $-47 \le h \le 31$ | $-42 \le h \le 46$ |
| | $-47 \le k \le 42$ | $-47 \le k \le 44$ | $-47 \le k \le 47$ | $-46 \le k \le 38$ |
| | $-15 \le l \le 28$ | $-18 \le l \le 28$ | $-28 \le l \le 28$ | $-28 \le l \le 27$ |
| reflections collected/unique | 49768/9522 | 53604/10767 | 54761/12699 | 52811/11438 |
| data/restraints/params | 9522/2409/854 | 10767/2332/904 | 12699/2371/904 | 11438/2314/859 |
| goodness-of-fit on $F^2$ | 1.015 | 1.050 | 0.965 | 1.076 |
| final *R* indices [$I > 2\sigma(I)$] | *R*1 = 0.0955, *wR*2 = 0.1535 | *R*1 = 0.0963, *wR*2 = 0.2449 | *R*1 = 0.0966, *wR*2 = 0.2427 | *R*1 = 0.0965, *wR*2 = 0.2357 |
| *R* indices (all data) | *R*1 = 0.3188, *wR*2 = 0.2031 | *R*1 = 0.1350, *wR*2 = 0.2899 | *R*1 = 0.1192, *wR*2 = 0.2659 | *R*1 = 0.1236, *wR*2 = 0.2638 |

**Table 3.** Crystal Data and Structure Refinement Parameters for Complexes of **5**−**8**

| | **5** | **6** | **7** | **8** |
|---|---|---|---|---|
| empirical formula | $C_{57}H_{54}N_{11}NdO_{18}$ | $C_{114}H_{110}N_{22}O_{37}Tb_2$ | $C_{114}H_{110}Dy_2N_{22}O_{37}$ | $C_{57}H_{54}ErN_{11}O_{19}$ |
| $M_r$ | 1325.35 | 2698.08 | 2705.24 | 1359.34 |
| crystal system | monoclinic | monoclinic | monoclinic | monoclinic |
| space group | *C*2/*c* | *C*2/*c* | *C*2/*c* | *P*2(1)/*n* |
| *a*/Å | 31.886(7) | 31.413(7) | 31.122(7) | 18.4100(3) |
| *b*/Å | 16.491(4) | 16.467(4) | 16.464(4) | 14.8252(2) |
| *c*/Å | 27.004(6) | 26.825(6) | 26.762(6) | 24.2554(4) |
| $\beta$/deg | 115.266(3) | 114.973(4) | 114.814(3) | 99.1440(10) |
| *V*/Å | 12842(5) | 12579(5) | 12447(5) | 6535.94(18) |
| *Z* | 8 | 4 | 4 | 4 |
| $D_c$ /kg m$^{-3}$ | 1.371 | 1.425 | 1.444 | 1.381 |
| $\mu$/mm$^{-1}$ | 0.884 | 1.202 | 1.279 | 1.360 |
| *F*(000) | 5416 | 5496 | 5504 | 2752 |
| crystal size/ mm | 0.45 × 0.41 × 0.39 | 0.35 × 0.16 × 0.08 | 0.21 × 0.17 × 0.14 | 0.32 × 0.23 × 0.19 |
| $\theta$ range for data collection/deg | 2.61−25.01 | 1.43−25.01 | 1.44−25.01 | 1.70−25.15 |
| index ranges, *hkl* | $-37 \le h \le 37$ | $-34 \le h \le 37$ | $-36 \le h \le 29$ | $-22 \le h \le 18$ |
| | $-19 \le k \le 19$ | $-19 \le k \le 19$ | $-19 \le k \le 19$ | $-17 \le k \le 13$ |
| | $-32 \le l \le 26$ | $-31 \le l \le 20$ | $-31 \le l \le 31$ | $-29 \le l \le 28$ |
| reflections collected/unique | 32299/11179 | 32545/11029 | 31248/10861 | 35561/12471 |
| data/restraints/params | 11179/222/784 | 11029/6/789 | 10861/6/789 | 11675/100/865 |
| goodness-of-fit on $F^2$ | 1.056 | 1.058 | 1.011 | 1.009 |
| final *R* indices [$I > 2\sigma(I)$] | *R*1 = 0.0432, *wR*2 = 0.1059 | *R*1 = 0.0568, *wR*2 = 0.1353 | *R*1 = 0.0658, *wR*2 = 0.1524 | *R*1 = 0.0381, *wR*2 = 0.0634 |
| *R* indices (all data) | *R*1 = 0.0772, *wR*2 = 0.1292 | *R*1 = 0.1233, *wR*2 = 0.1832 | *R*1 = 0.1544, *wR*2 = 0.2141 | *R*1 = 0.0923, *wR*2 = 0.0997 |

## Results and Discussion

**Synthesis.** Both tetrapodal ligands $L^I$ and $L^{II}$ were prepared by the ether base coupling of Pentaerythritol benzenesulfonate and the appropriate salicylamide in a 1:4 ratio in dry DMF in the presence of an excess of anhydrate $K_2CO_3$. The precursor Pentaerythritol benzenesulfonate and salicylamide were prepared in excellent yield from Pentaerythritol and methyl salicylate, respectively, according to the literature procedure.[16,17] Purification of $L^I$ was accomplished by column chromatography over silica, eluting with petroleum ether + ethyl acetate(v/v = 10:1) to give a pale white solid with the yield of 87%, and $L^{II}$ was purified by column chromatography over silica, eluting with petroleum ether + ethyl acetate(v/v = 5:1) to give a pale white solid with the yield of 48%.

One of the important issues in determining the framework structures is the geometry of the organic ligands. In our study, the terminal coordinating donors are separated by the quarternary carbon atom at the tetrahedral position, and four salicylamide arms are rotationally free and are thus capable of adjusting to match well the metal coordination preference. The structural difference between the two ligands is the aromatic ring in the salicylamide terminal groups. These two new ligands gave satisfactory $^1$H NMR, IR spectra, mass spectrometry, and elemental analyses. Treatment of $Ln(NO_3)_3 \cdot 6H_2O$ with the two ligands in ethyl acetate-methanol solution yields a series of complexes which, according to combustion analysis, correspond to the formula of $Ln_4L^I_3(NO_3)_{12}(C_4H_{10}O)_3$ (Ln = Pr, Er), $Ln_4L^I_3(NO_3)_{12}(C_4H_{10}O)_6$ (Ln = Eu, Tb), $Ln_2L^{II}_2(NO_3)_6(H_2O)_n$ (Ln = Nd, Tb, Dy, $n$ = 2 or 3) and $ErL^{II}(NO_3)_6(H_2O)_2$, respectively.

(18) (a) Sheldrick, G. M. *SHELXL-97, Program for the Solution of Crystal Structures*; University of Göttingen: Göttingen, Germany, 1997. (b) Sheldrick, G. M., *SHELXL-97, Program for the Refinement of Crystal Structures*; University of Göttingen: Göttingen, Germany, 1997.

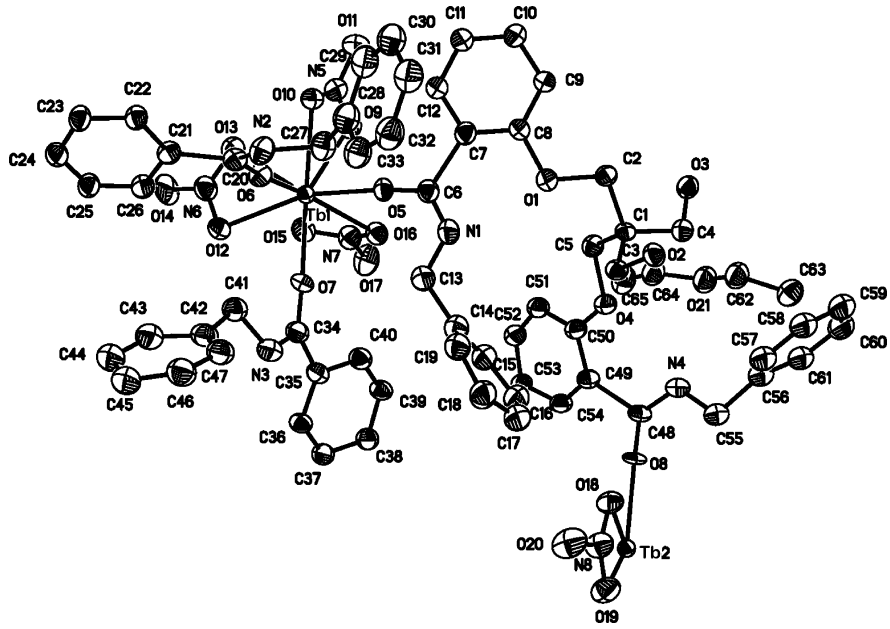


**Figure 1.** Oak Ridge Thermal Ellipsoid Plot (ORTEP) of complex **3** showing the local coordination environment of $Tb^{III}$ with thermal ellipsoids at 30% probability (crystalline solvent molecules are omitted for clarity).

X-ray quality crystals of all the complexes were obtained after several weeks from vapor diffusion from ethyl acetate-methanol solution. The complexes are soluble in DMF, DMSO, methanol, and ethanol, slightly soluble in ethyl acetate, acetonitrile and acetone, but insoluble in $CHCl_3$ and ether.

**IR Spectra Analyses.** The characteristic band of the carbonyl group of free ligand $L^I$ and $L^{II}$ is shown at 1650 $cm^{-1}$ and 1638 $cm^{-1}$, respectively. The absence of the band round 1650 $cm^{-1}$, which is instead of a new band at 1604 $cm^{-1}$ of the $L^I$ complex compared to free ligand, indicates the complete coordination of the ligand, while the IR spectrum of the $L^{II}$ complex confirmed the presence of both the uncoordinated and coordinated carbonyl group with a peak at about 1638 $cm^{-1}$ and 1603 $cm^{-1}$. This suggests that the lanthanide ions exert considerable more influence on $\nu$(C═O) values of ligand $L^I$ than that of ligand $L^{II}$. Weak absorptions observed in the range of 2900−2950 $cm^{-1}$ can be attributed to the $\nu(CH_2)$ of the ligand. The broad bands at about 3402 $cm^{-1}$ are ascribed to the vibration of the water ligands in the $L^{II}$ complexes.

**Structure Description. Structure I.** Prismatic crystals of **1**−**4** were obtained by reaction of $Ln(NO_3)_3 \cdot 6H_2O$ and $L^I$ in a 1:1 mol ratio in methanol-ethyl acetate solution. They are air stable and have a similar thermal decomposition behavior, which is reasonable since they possess the same polymeric motif. X-ray crystal structure analyses reveal that **1**−**4** are isostructural and crystallize in the high-symmetry space group *R*3*c*, differing only slightly by crystalline solvents and a slight contraction of the Ln coordination sphere as expected; therefore, details will only be provided for the Tb analogue, **3**. Because no ether was directly introduced to the starting reaction mixture, the crystalline ether might be derived from ethyl acetate. In an asymmetric unit, there are three ligands $L^I$ and four crystallographically independent $Ln^{3+}$ ions (M = Pr, Eu, Tb, and Er) which can be classified into two different types on the basis of their coordination environment, and the ratio of Tb1/Tb2 is 3:1. Tb1 shows the nona-coordinated monocapped tetragonal antiprism geometry, completed by three crystallographically different carbonyl O atoms (O5, O6, O7) from three different ligands and six nitrate O atoms (O9, O10, O12, O13, O15, O16), whereas Tb2 owns the same coordinate geometry as Tb1 and bonds to three crystallographically equal carbonyl O atoms (O8) of three different ligands and six nitrate O atoms (O18, O19). The Tb−Onitrate bond lengths span the range of 2.436(3)−2.570(3) Å, but the Tb−Ocarbonyl bond lengths obviously vary from 2.264(3) to 2.771(3) Å, both of which are comparable with those observed in other $Tb^{III}$-containing coordination polymers[19] (Figure 1).

The general trend of decreasing Ln−O distance in the series $Pr^{3+} > Eu^{3+} > Tb^{3+} > Er^{3+}$ is in agreement with the lanthanide contraction and reflects a decrease in ionic radii: 1.13 > 1.08 > 1.05 > 1.03 Å[20] (Supporting Information, Table S1−S4). Each ligand was bonded to four nona-coordinated $Tb^{III}$ ions, via complexation by carbonyl oxygen donors on salicylamide arms. The $Tb^{III}$ ions in turn coordinated to three salicylamide arms of three other adjacent ligands, meaning that each ligand was linked by Tb coordination to four adjacent ligands. The above three-dimensional (3D) structure can also be explained by considering smaller building units. Thus, the Tb1 polyhedron units are connected through $\mu$3 Tb2 polyhedron units in 3D directions, forming a tetrahedron tetramer. The tetrahedron tetramers are, again, connected to three Tb1 polyhedron units

(19) (a) Wan, Y.; Jin, L.; Wang, K.; Zhang, L.; Zheng, X.; Lu, S. *New J. Chem.* **2002**, *26*, 1590. (b) Liu, C. B.; Sun, C. Y.; Jin, L. P.; Lu, S. Z. *New J. Chem.* **2004**, *28*, 1019. (c) Sun, H. L.; Gao, S.; Ma, B. Q.; Chang, F.; Fu, W. F. *Microporous Mesoporous Mater.* **2004**, *73*, 89. (d) Reineke, T. M.; Eddaoudi, M.; Fehr, M.; Kelley, D.; Yaghi, O. M. *J. Am. Chem. Soc.* **1999**, *121*, 1651.

(20) Cotton, F. A.; Wilkinson, G.; Murillo, C. A.; Bochmann, M., *Advanced Inorganic Chemistry*, 6th ed.; John Wiley & Sons: New York, 1999; p 1109.

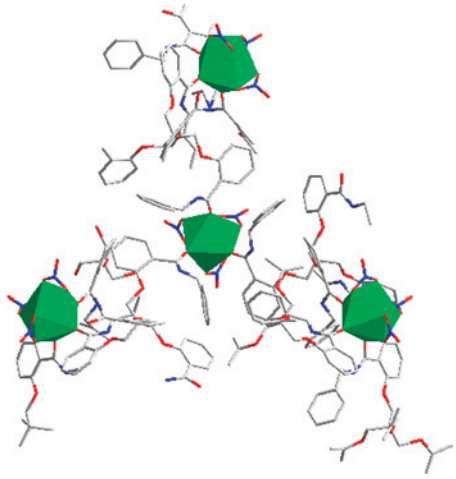

**Figure 2.** View of the tetramer of complex **3** showing the formation process of the 3D interpenetration coordination polymers.

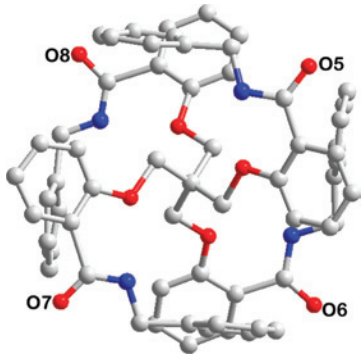


**Figure 3.** Ligand $L^I$ in complex **3** showing a circular fashion.

which are, again, connected through $\mu$3 Tb2 polyhedron units in 3D directions, forming a hexadecamer; in this way, the 3D interpenetration coordination is formed (Figure 2).

It is interesting to note that the ligands $L^I$ were arranged with all four salicylamide arms in a circular fashion (Figure 3), each salicylamide arm had a similar conformation, and the arm is so long that their terminal groups can "fold back". Four oxygen atoms of the carbonyl groups in the ligand, namely, O5, O6, O7, and O8, are located in the outer part of the whole ligand molecule. This conformation is necessary for the ligand to bind four $Tb^{III}$ ions simultaneously. Overall, the ligands in all four complexes were arranged in virtually identical fashion, with most of the differences due to slight changes in folding at the -$CH_2$ groups or small rotations of the C−C bonds. These changes were probably caused by the overall framework having to accommodate lanthanide ions ranging in size from the large Nd to the small Er.

Better insight into this framework can be achieved by the application of a topological approach, reducing multidimensional structures to simple node and connection nets. As discussed above, in this framework, each nona-coordinated $Tb^{3+}$ ion is linked with three ligands through carbonyl groups, which could be considered as an inorganic trigonal node with short topological terms of $8^3$. Each $L^I$ ligand in turn is connected with four $Tb^{3+}$ ions through carbonyl groups, so it could be regarded as an organic tetrahedron linker. There are three eight-membered rings around the three-connected metal node, while six eight-membered rings

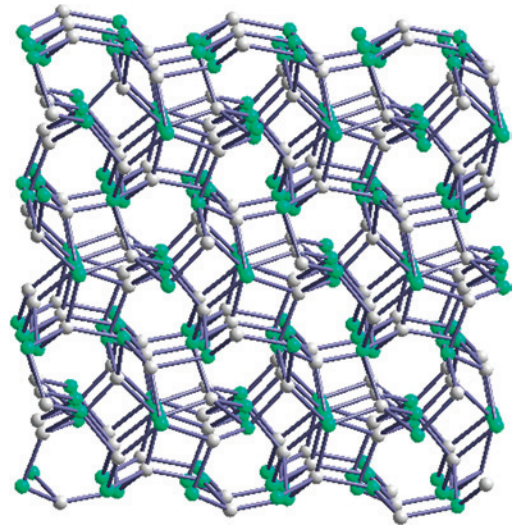

**Figure 4.** Topological representation of the (3,4)-connected $(8^3)_4(8^6)_3$ net in the coordination polymer of $L^I$ (the connectors of ligand $L^I$ and Tb atoms are colored gray and green, respectively).

are around the four-connected linker, resulting in a ligand linker topology of $8^6$. Because the three-connected nodes and four-connected linkers are arranged in a ratio of Tb/L = 4:3, the short Schläfli symbol of the topology can be expressed as $(8^3)_4(8^6)_3$ (Figure 4). Thus, a novel interpenetrating network based upon the binodal pyramidal 3,4-connected nodes has been generated, which is among the rare 3D nets with topology of a $(8^3)_4$ $(8^6)_3$ notation and unprecedented in lanthanide complexes of salicylamide ligands.

**Structure II.** To confirm the role of different terminal groups in the self-assembly process, $L^{II}$ was used instead of $L^I$ to perform the reaction. X-ray structural analyses revealed that the Nd, Tb, and Dy complex of ligand $L^{II}$ formed isomorphous crystal structures which crystallized in the monoclinic space group $P2_1/c$ with two carbonyl O-atoms remaining uncoordinated which probably is due to the existence of pyridyl nitrogen atoms. Representative bond lengths and angles are listed in Supporting Information, Table S5−S7. Therefore the structure of complex **5** was described in detail to introduce the structure II. Compound **5** shows a dinuclear structure with the asymmetric unit containing one crystallographically unique $Nd^{3+}$ ion, one neutral ligand, three bidentate nitrates, and one water molecule. A view of the molecular structure, together with its numbering scheme, is depicted in Figure 5. The neodymium(III) atom is in a distorted [NdO9] monocapped square antiprismatic coordination geometry, of which the coordination sphere for $Nd^{III}$ is defined by two carbonyl oxygens (Nd−O = 2.373(3) Å, 2.380(3) Å) from two different ligands $L^{II}$, six nitrate oxygen atoms (Nd−O = 2.497(4) Å, 2.497(4) Å, 2.500(4) Å, 2.518(3) Å, 2.525(4) Å, 2.641(3) Å), and one water molecule (Nd−O = 2.417(3) Å).

Two arms of $L^{II}$ ligands arrange in a complementary head-to-head fashion to bind two neodymium atoms into a distorted 28-membered binuclear ring with the other two uncoordinated arms dangling freely, in which there is only one inversion center (*i*) without any crystallographically imposed symmetry for the ligands or the metal centers

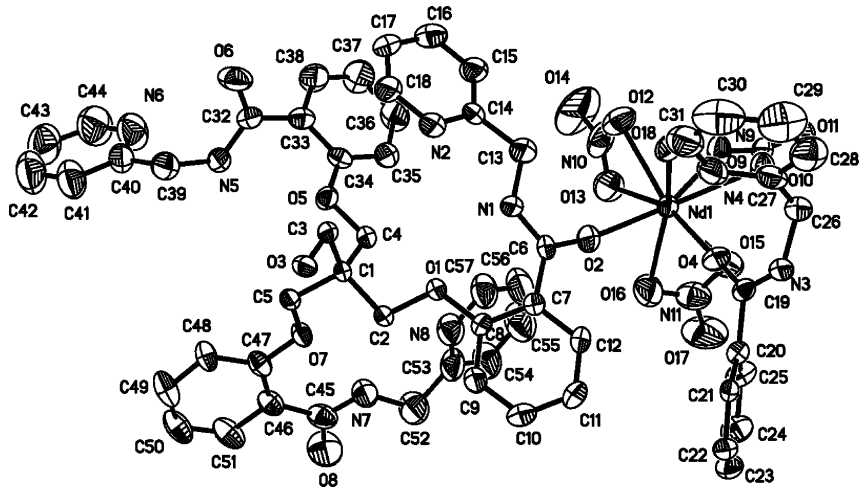


**Figure 5.** ORTEP plot of complex **5** showing the local coordination environment of $Nd^{III}$ with thermal ellipsoids at 30% probability.

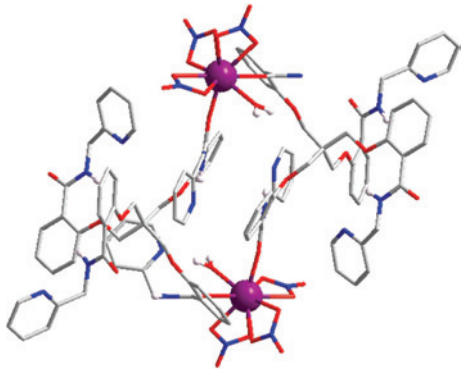

**Figure 6.** Cage-like homodinuclear structure of complex **5**.

(Figure 6). This gives rise to a Nd···Nd distance of 12.750(3) Å.

It is well-known that the most important driving forces in crystal engineering are coordination-bonding and hydrogen-bonding interactions. Extended networks assembled by both coordination and hydrogen bonds are one of the important strategies to construct supramolecular networks.[21] In principle, higher dimensionality networks can be obtained by the assembly of lower dimensionality polymers (or molecules) via hydrogen bonding interactions. A series of such compounds, was reported before.[22]

Notably, significant intra- and intermolecular hydrogen bonding interactions exist between the cage-like dimers which are the most important factor preventing complexes **5**−**7** from assembling into infinite coordination polymers. First, the cage-like dimers are held together into one-dimensional (1D) supramolecular chains via hydrogen bonding between uncoordinated carbonyl oxygen atoms and amide nitrogen atoms (Figure 7). The N5···O8 distance (2.795(5) Å) and N5−H5···O8 angle (156.71°) are both within the ranges of those reported hydrogen bonds. Further, the other uncoordinated carbonyl oxygen atoms can interact with the oxygen atoms of the coordinated water in two directions to form an interesting 3D supramolecular structure with the O18···O6 distance of 2.658(5) Å and O18−H61···O6 angle of 158.32° (Figure 8). It is remarkable that these inter- and intramolecular hydrogen bonds are the most important factors preventing complexes **5**−**7** from assembling into infinite coordination polymers, which is quite different from the complexes of ligand $L^{I}$.

**Structure III.** The programming of helicates containing two or three d transition metal ions is relatively easy in view of the substantial steric requirements of these ions. On the other hand, trivalent 4f ions have their valence orbitals shielded by the $5s^25p^6$ filled subshells and display, therefore, less specific steric requirements. It is reported that reduction of the denticity of one coordinating group yields receptors able to incorporate simultaneously a d and a 4f transition metal ion into the helical edifices;[23] besides the large body of data they have published on f-f and d-f helicates, only few other lanthanide-containing helicates have been reported based on other ligand design.

Even though the radius of $Er^{III}$ is only 0.026 Å smaller than that of $Dy^{III}$, the introduction of Er during the synthesis results a quite different product which exhibits a single-strand helical chain structure winding around a $2^1$ axis. As shown in Figure 9, each $Er^{III}$ center adopts a ($ErO_9$) nona-coordination sphere that consists of one water donor, three bidentate nitrates, and two carbonyl donors from two different $L^{II}$ ligands. Among them, one oxygen atoms O11 is from water, and the Er−O bond length is 2.305(3) Å; six oxygen atoms (O9, O11, O12, O14, O15 and O17) are from the bidentate nitrate groups, and the Er−O bond lengths are 2.432(3), 2.421(4), 2.412(3), 2.446(3), 2.426(3), and 2.470(3) Å, respectively; the other two oxygen atoms O(2) and O(8) are from carbonyl groups, and the Er−O bond lengths are 2.302(3) and 2.281(3) Å, respectively. All of the bond lengths for Er−O fall into normal ranges (Supporting Information, TableS8).

The $Er^{III}$ complex of ligand $L^{II}$ comprises an infinite neutral single-strand helix, rather than a dinuclear complex, which is constituted from the alternate linkage of $Er^{III}$ cations and ligands $L^{II}$ with stoichiometry $ErL^{II}(NO_3)_3$, and each helical pitch contains two $Er^{III}$−L units (Figure 10). The helical pitch, given by the distance between equivalent atoms generated by one full rotation of the 2-fold screw axis, is

(21) Beatty, A. M. *Coord. Chem. Rev.* **2003**, *246*, 131.

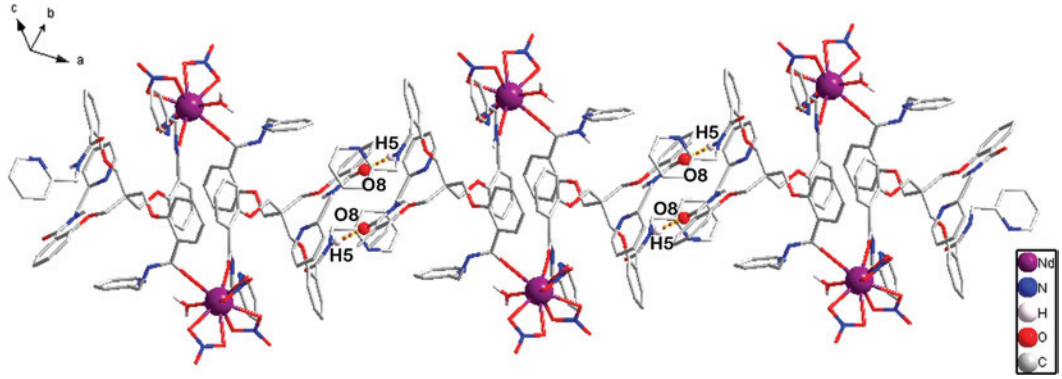


**Figure 7.** 1D supramolecular chains of **5** constructed by hydrogen bonding between uncoordinated carbonyl oxygen atoms and amide nitrogen atoms which are indicated with dashed orange lines.

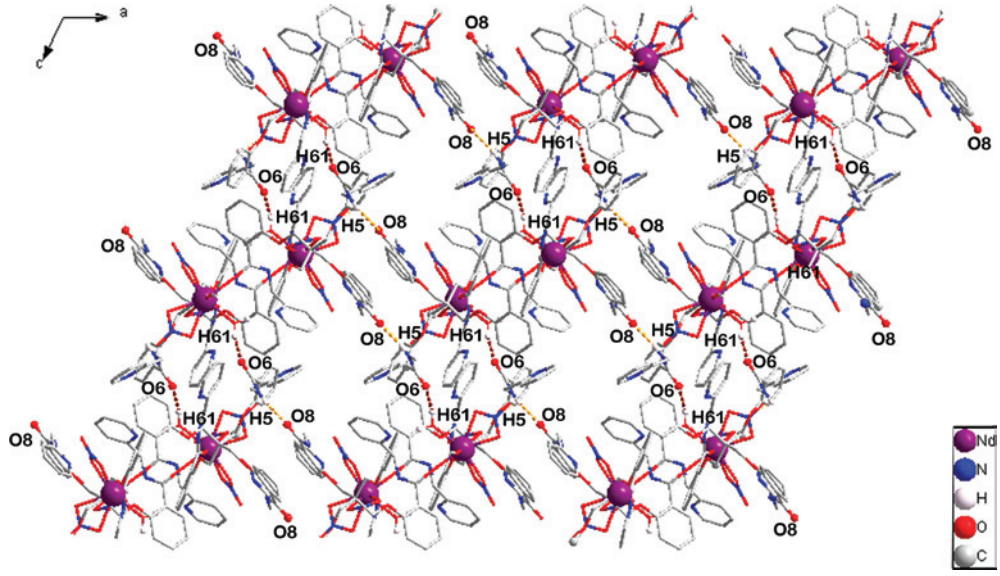


**Figure 8.** 3D supramolecular chains of **5** constructed by hydrogen bonding which are indicated with dashed orange lines.

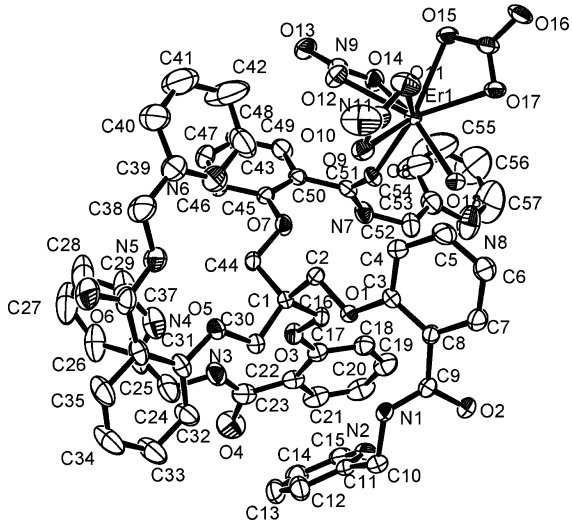


**Figure 9.** ORTEP plot of complex **8** showing the local coordination environment of $Er^{III}$ with thermal ellipsoids at 30% probability.

14.83 Å. The $Er^{III}$ atom adopts an almost monocapped antisquare prism coordination geometry while $L^{II}$ acts as a bidentate bridging ligand with only two of its amidic oxygen atom interacting with the $Er^{III}$. The right-handed and left-handed helixes co-exist in each $Er^{III}$ complex, and they are arrayed in an alternate fashion to generate a racemic crystal. The lattice water molecules are supported by the pyridine N atom via H-bonds, with O···O distances of about 2.93 Å.

It is worth noting that the O4 and O6 atoms of $L^{II}$ are not coordinated to the $Er^{III}$ center either, similar to complexes **5**−**7**, which presents strong intermolecular hydrogen bonding interactions with the amide nitrogen N7 and N1 atoms in different directions forming a 3D supramolecular structure with a O4···N7 separation of 2.699(3) Å and a O6···N1 separation of 2.833(3) Å, respectively (Figure 11).

**Comparison of the Structures.** In the investigations of the self-assembly between lanthanide nitrate salts and two structure-related tetrapodal ligands, eight novel crystal products were isolated, and three types of structures were obtained. In the three types of structures, the coordination number (CN) of the $Ln^{III}$ ion is nine, and the $Ln^{III}$ ion is located in the distorted monocapped square antiprism. We can see that the cell parameter values of *a*, *b*, *c*, and *V* decreased with an increase in the atomic number for structures I from Table 2. In complexes **1**−**4**, the Ln−O average bond lengths decreased from 2.377 to 2.293 Å (Ln−Ocarbonyl) and from 2.530 to 2.436 Å (Ln−Onitrate) with an increase in atomic number. In the same way in complexes **5**−**8**, the bond average length of Ln−Ocarbonyl,

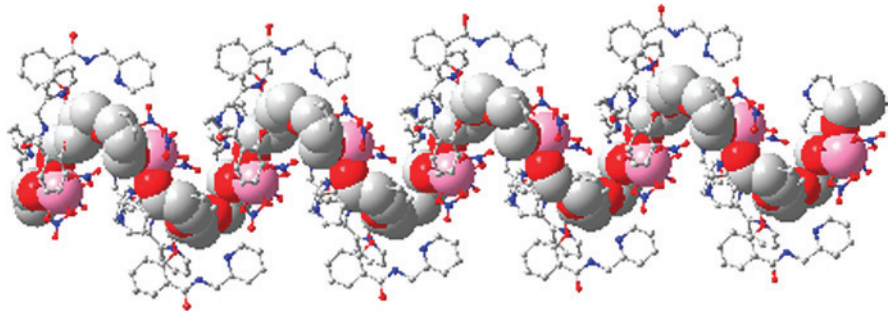

**Figure 10.** View of the 1D infinite neutral coordination single-strand helix of **8**.

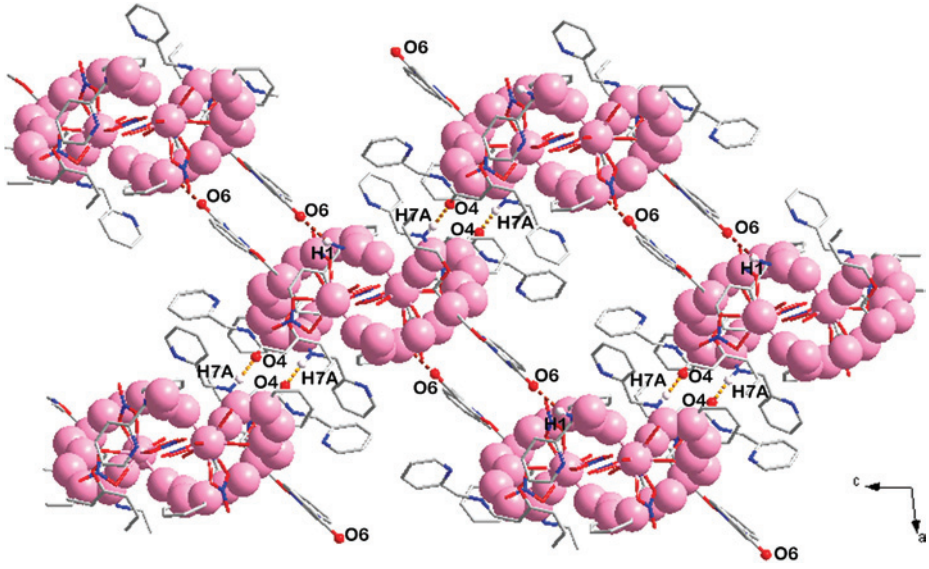


**Figure 11.** 3D supramolecular chains of **8** (viewing along *b*-axis) constructed by hydrogen bonding which are indicated with dashed orange lines.

Ln−Onitrate, and Ln−Owater also decreased with an increase in the atomic number. All these should be ascribed to the lanthanide contraction effect together with the structure transformation form structures II to structure III. It is likely that hydrogen bonding by the nitrogen atoms of terminated pyridine to coordinated water subunits subtly contorts the conformation of the aliphatic tether in **5**−**8**. Furthermore, the crystal system and space group for structure II were triclinic and $P2_1/c$ as well as monoclinic and $P2_1/n$ for structure III.

It is important to note that the etheric oxygen atoms of the two ligands are not coordinated to the $Ln^{III}$ center, but act as the hydrogen bonding acceptors to form strong intramolecular N−H···O hydrogen bonds which are stabilized by a stable 6-membered ring. The binding of lanthanide ions to the carbonyl oxygen atoms of ligands rather than to etheric oxygen groups appears largely as a consequence of the cooperative effect of strong intramolecular hydrogen bonds and steric hindrance inhibiting the formation of a reasonable coordination geometry that involves the participation of all four ether oxygen donors of each ligand. In any case, a number of etheric oxygen-containing amide ligands have been documented previously[24] to exhibit strong affinities for lanthanide.

This type of terminal group-depending structural variation can be understood taking into account the plastic coordinative behavior of the ligand, modulated by the introduction of more electronegative pyridyl nitrogen atoms at the aromatic salicylamide arms. Compared with $L^I$, the coordination behavior of $L^{II}$ was dramatically changed because of the presence of four pyridine nitrogen atoms which could make it more favorable for incorporating hydrogen bonds and affecting the coordination mode of the resulting tetrapodal ligand. Consequently, each $L^{II}$ ligand keeps half of its salicylamide arms free from coordinating, and the dimensionality is much lower than those of the $L^I$ ligand. The formation of a 3D interpenetrating network takes place in a terminal group which has a weaker hydrogen bond acceptor, allowing the coordination of $Ln^{III}$ simultaneously by the four salicylamide arms of the ligands and thus the assembly of the rare 3D nets with topology of a $(8^3)_4$ $(8^6)_3$ notation. On

(22) (a) Carlucci, L.; Ciani, G.; Proserpio, D. M.; Sironi, A. *J. Chem. Soc., Dalton Trans.* **1997**, 1801. (b) Dong, Y.-B.; Smith, M. D.; Layland, R. C.; Loye, H.-C. *J. Chem. Soc., Dalton Trans.* **2000**, 775.

(23) (a) Jensen, T. B.; Scopelliti, R.; Bünzli, J.-C. G. *Inorg. Chem.* **2006**, *45*, 7806. (b) Albrecht, M; Osetska, O.; Fröhlich, R.; Bünzli, J.-C. G.; Aebischer, A.; Gumy, F.; Hamacek, J. *J. Am. Chem. Soc.* **2007**, *129*, 14178.

(24) (a) Guo, Y.-L.; Dou, W.; Liu, W.-S.; Wang, D.-Q. *Polyhedron* **2007**, *26*, 1699. (b) Wang, Y.-W.; Liu, W.-S.; Yu, K.-B. *Anorg. Allg. Chem.* **2006**, *632*, 482. (c) Tang, K.-Z.; Zhang, J.; Tang, Y.; Liu, W.-S.; Tan, M.-Y.; Sun, Y.-X. *Inorg. Chim. Acta* **2005**, *8*, 1018. (d) Lei, K.-W.; Liu, W.-S.; Tan, M.-Y. *Spectro. Acta Part A.,* **2007**, *66*, 118. (e) Matloka, K.; Gelis, A.; Regalbuto, M.; Vandegriftb, G.; Scott, M. J. *Dalton Trans.,* **2005**, 3719. (f) Li, X. F.; Liu, W. S.; Guo, Z. J.; Tan, M. Y. *Inorg. Chem.,* **2003**, *42*, 8735.

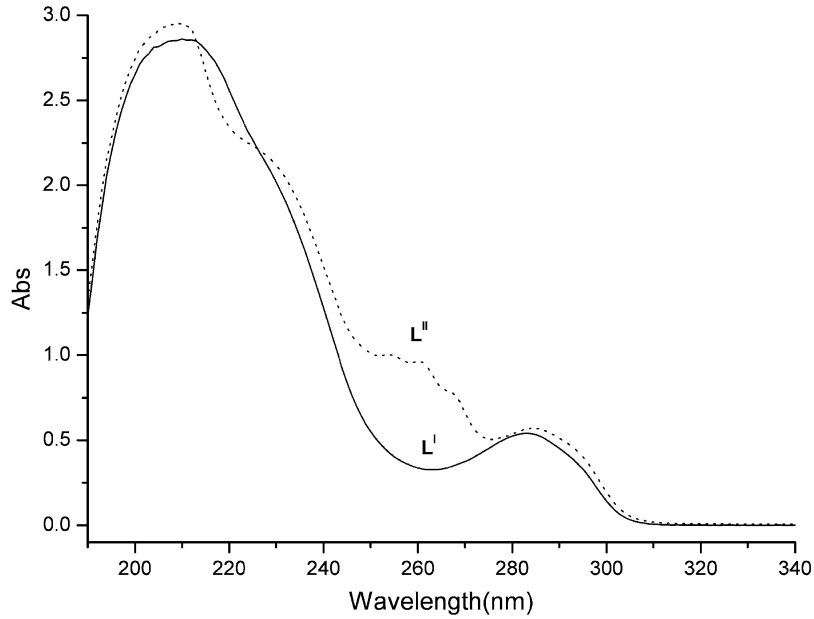


**Figure 12.** Electronic spectra of ligand $L^I$ and $L^{II}$ in acetonitrile solution ($6.8 \times 10^{-4}$ M).

the other hand, the more electronegative pyridine nitrogen atoms of ligand $L^{II}$ play the dominant role in the adjustment of the coordination modes of the tetrapodal ligands through strong intramolecular hydrogen bonding interactions and results in the formation of low-dimensional coordination complexes with two arms of ligand $L^{II}$ uncoordinated which further effect the luminescence properties as compared to those of ligand $L^I$.

**Photophysical Properties of Ligands and of Their Complexes. Photophysical Properties of the Ligand.** In acetonitrile, the absorption spectra of the ligand $L^I$ (Figure 12) features two main bands located around 210 ($\varepsilon$/dm$^3$ mol$^{-1}$ cm$^{-1}$, 4207) and 285 nm ($\varepsilon$/dm$^3$ mol$^{-1}$ cm$^{-1}$, 797) which could be assigned to characteristic $\pi-\pi^*$ transitions centered on the salicylamide units. The main difference of the UV-vis absorption spectrum between the two ligands is the presence of characteristic $\pi-\pi^*$ transitions centered on the pyridine ring in the absorption spectra of the ligand $L^{II}$. So we can draw the conclusion that the aromatic terminal groups do not affect the electronic properties of the salicylamide moiety considerably. The titration of $Ln^{3+}$ was also carried out by adding aliquots of $Ln(NO_3)_3$ acetonitrile solution into the acetonitrile solutions containing ligands $L^I$ and $L^{II}$. During the titration, the UV−vis spectra showed negligible changes. This suggests no significant change in the overall electronic structure of the ligands upon addition of $Ln^{3+}$.

However, the large molar absorption coefficient of the ligands indicates favorable conditions for an efficient antenna effect. Excited by the absorption band at 305 nm, the two ligands display only a strong luminescence band around 450 nm. The ligand-centered luminescence in the $Gd^{III}$ complex displays basically the same features observed in the free ligand, thus confirming the suitability of this ligand as a sensitizer for $Eu^{III}$ and $Tb^{III}$ luminescence.

It is well-known that the energy transfer from ligand excited states to the resonance states of $Ln^{III}$ in complexes can occur in different ways. The favored simplified mechanism involves ligand excitation by the absorption of ultraviolet energy to an excited singlet state, followed by energy migration via nonradiactive intersystem crossing to a ligand triplet state (E1 = $E$(S1 − $T_{0-0}$)), and energy transfer from the triplet state to a resonance state of the $Ln^{III}$ ion, from which the emission occurs (E2 = $E(T_{0-0}) - E$).[25]

To demonstrate the energy transfer process, luminescence measurements in a solid matrix (MeOH) performed at 77 K enable the observation of phosphorescence of the ligand ($T_{0-0}$ state). For the Gd(III) complex of ligand $L^I$, upon cooling to 77 K, an intense unstructured emission band appeared from 370 to 550 nm (Supporting Information, Figure S1), which can be attributed to phosphorescence from the ligand $T_{0-0}$ state. As detailed elsewhere, the lowest $T_{0-0}$ energy was estimated by spectral deconvolution of the 77 K luminescence signal into several overlapping Gaussian functions (Supporting Information, Figure S1).[26] The resulting $T_{0-0}$ energy was evaluated to be about 24 096 cm$^{-1}$. For the Gd(III) complex of ligand $L^{II}$ the emission band appeared from 391 to 550 nm (Supporting Information, Figure S2) and the resulting $T_{0-0}$ = 23 474 cm$^{-1}$. The energetic position of the triplet state of ligand $L^{II}$ is about 622 cm$^{-1}$ lower in energy than that of ligand $L^I$ which also demonstrates slightly the terminal effect.

**Luminescence Properties of the Complexes in the Solid State.** To examine the ability of the ligands to be antenna groups for sensitized luminescence from lanthanides, we measured the luminescence properties of the $Eu^{III}$, $Tb^{III}$ complex with the two ligands. The excitation spectra recorded upon metal-centered emission of the $Tb^{III}$ complex in solid state (Figure 13) overlaps the absorption spectrum in the region between 280−310 nm, indicating that the L → Ln energy transfer goes through the triplet state. The

(25) (a) Sabbatini, N.; Guardigli, M.; Lehn, J.-M. *Coord. Chem. Rev.* **1993**, *123*, 201. (b) Bünzli, J.-C. G. *J. Alloys Compd.* **2006**, *408*−*412*, 934.
(26) Moore, E. G.; Xu, J.; Jocher, C. J.; Castro-Rodriguez, I.; Raymond, K. N. *Inorg. Chem.* **2008**, *47*, 3105.

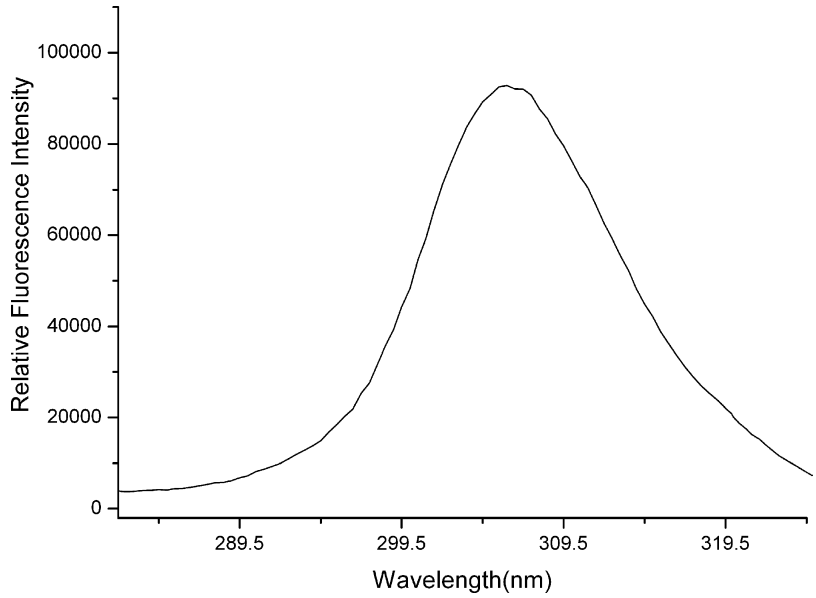


**Figure 13.** Room-temperature excitation spectra for the $Tb^{III}$ complex of ligand $L^I$ in solid state ($\lambda_{em}$ = 490 nm, excitation and emission passes = 1 nm).

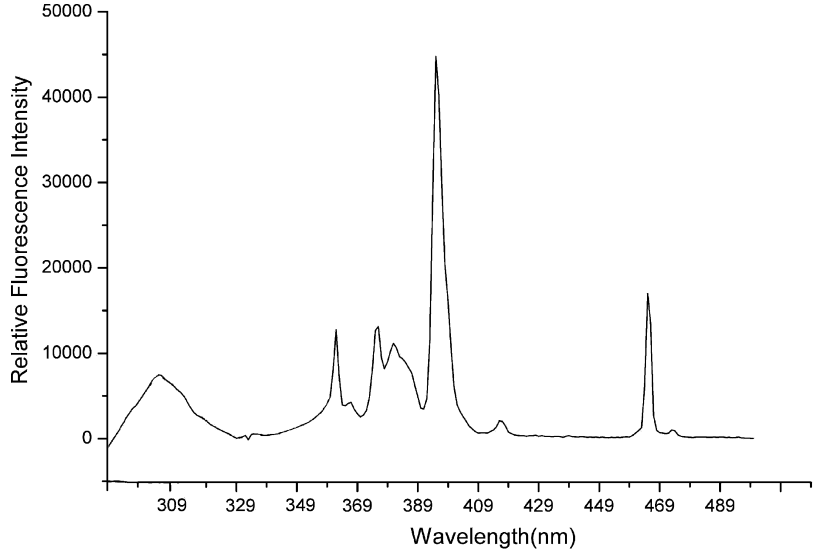


**Figure 14.** Room-temperature excitation spectra for $Eu^{III}$ complex of ligand $L^I$ in solid state ($\lambda_{em}$ = 579 nm, excitation and emission passes = 2.5 nm).

excitation spectrum of the europium complex of these two ligands (Figure 14) monitoring the emission wavelength at 579 nm exhibits a series of sharp lines characteristic of the $Eu^{III}$ energy-level structure, which indicates that the Eu luminescence is not efficiently sensitized and which is quite different from $Tb^{III}$ complexes.

The luminescence spectra of the $Eu^{III}$ complex display a mixture of ligand-centered band emission and metal-centered line emissions as shown in Figure 15. The emission peaks of the $Eu^{III}$ complex at 579, 592, 619, 687, and 695 nm can be assigned to $^5D_0 \rightarrow {}^7F_J$ ($J$ = 0, 1, 2, 4) transitions of the $Eu^{III}$ ion, respectively. Notably, the $^5D_0 \rightarrow {}^7F_2$ transition is much more intense than the $^5D_0 \rightarrow {}^7F_1$ transition, the large intensity ratio of $Eu^{III}$ complex for $I(^5D_0 \rightarrow {}^7F_2)/I(^5D_0 \rightarrow {}^7F_1)$ indicates the absence of an inversion center at the $Eu^{III}$ site which is in agreement with the result of single crystal X-ray analysis. The fluorescence quantum yield $\Phi$ of the europium nitrate complex in solid state was found to be 6.5 ± 0.1% using an integrating sphere. The Eu complex luminescence decay is best described by a double-exponential process with significantly longer lifetimes of $\tau 1$ = 1.315 ± 0.001 ms, $\tau 2$ = 0.340 ± 0.001 ms observed and may be due to the presence of two distinct emitting species (Supporting Information, Figure S3).

When $Tb^{III}$ is introduced into the edifices of ligand $L^I$ (Figure 16), as with the europium spectra, the dominant peak is the hypersensitive transition, $^5D_4 \rightarrow {}^7F_5$, which is made up of a single intense peak with a shoulder at approximately one-third intensity at lower frequency. The $^5D_4 \rightarrow {}^7F_6$ is the second largest peak observed. The $^5D_4 \rightarrow {}^7F_4$ and $^5D_4 \rightarrow {}^7F_3$ transitions consist of two peaks. The ligand fluorescence disappears completely indicating a very efficient energy transfer from ligand to $Tb^{III}$ center. This result is consistent with the work of Latva et al.,

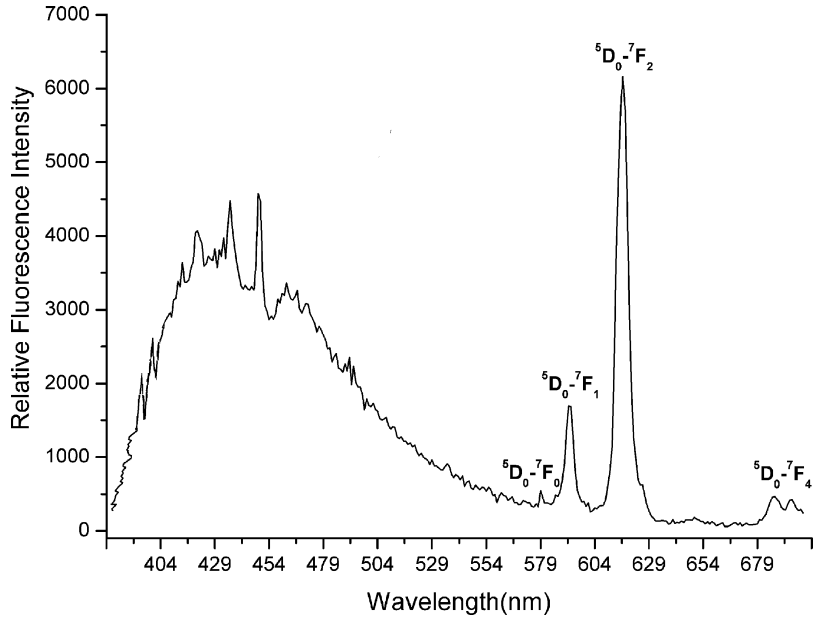


**Figure 15.** Room-temperature emission spectra for the $Eu^{III}$ complex of ligand $L^I$ in solid state ($\lambda_{ex}$ = 397 nm, excitation and emission passes = 2.5 nm).

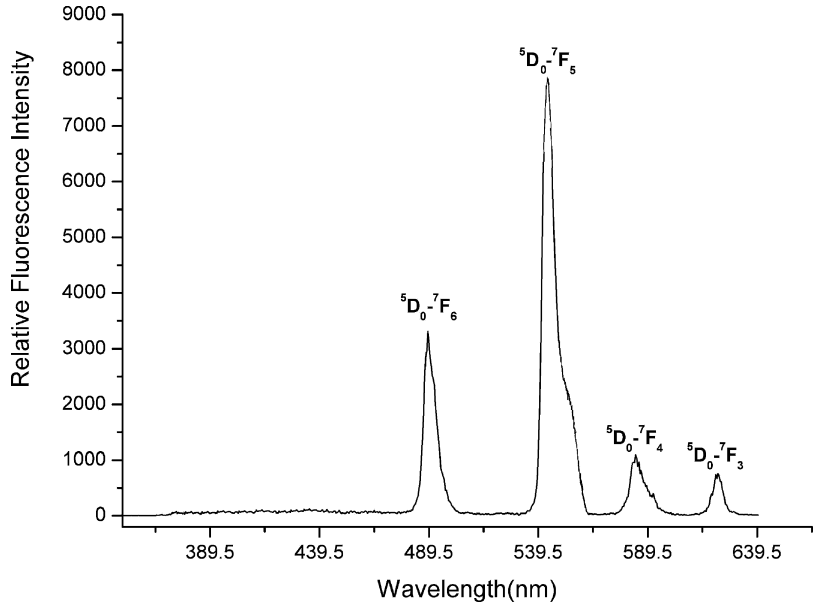


**Figure 16.** Room-temperature emission spectra for the $Tb^{III}$ complex of ligand $L^I$ in solid state ($\lambda_{ex}$ = 305 nm, excitation and emission passes = 1 nm).

who suggested that a fast and irreversible energy transfer to the $Tb^{III}$ ion occurs when an energy gap, E2 ($E$(T) − $E$($^5D_4$)), is greater than 1850 $cm^{-1}$.[27] The fluorescence quantum yield Φ of the terbium nitrate complex in solid state was found to be 27.6 ± 0.1% using an integrating sphere at room temperature. The Tb complex luminescence decay is best described by a double-exponential process with significantly longer lifetimes of $\tau 1 = 2.634 \pm 0.001$ ms, $\tau 2 = 1.823 \pm 0.001$ ms observed likely because of the presence of two distinct emitting species (Supporting Information, Figure S4). The relatively long luminescence lifetimes are an indication that the tetrapodal ligand provides a significant level of protection from non-radiative deactivation of the lanthanide cations which is consistent with the single crystal analysis.

In contrast to the $Eu^{III}$ and $Tb^{III}$ complex of ligand $L^I$, the quantum yield (8.1 ± 0.1% for $Tb^{III}$ complex; 1.2 ± 0.1% for $Eu^{III}$ complex) and the lifetimes (1.214 ± 0.001 ms for $Tb^{III}$ complex; 0.594 ± 0.001 ms for $Eu^{III}$ complex) of $Eu^{III}$ and $Tb^{III}$ complex of ligand $L^{II}$ are smaller or shorter than that of ligand $L^I$ accordingly suggesting one or more non-radiative pathways are assisting in the deactivation of the excited state and shortening the observed lifetimes, for the triplet energy level of the antenna only changed slightly with the terminal group, which excludes the possibility that the quenching of

(27) Latva, M.; Takalo, H.; Mukkala, V.-M; Matachescu, C.; Rodriguez-Ubis, J.-C.; Kankare, J. *J. Lumin.* **1997**, *75*, 149.

luminescence is due to a change of the nature of the antenna triplet state. It is well-known that the presence of OH oscillators in the lanthanide first coordination sphere provides an efficient non-radiative path,[28] so we can suggest that the observed decrease in the lifetime of the $^5D_4$ level and the $^5D_0$ level is mainly related to an increase in non-radiative transitions due to the increase in the number of OH oscillators in the $Tb^{III}$ or $Eu^{III}$ first coordination shell of ligand $L^{II}$, which is in perfect agreement with the proposed structural results. It is also interesting that although the tetrapodal ligand $L^{II}$ does not shield $Tb^{3+}$ using all four arms, its Tb complex is still highly luminescent. It is worth noting that the luminescence decays of complexes of ligand $L^{II}$ show an obvious single-exponential decay behavior in solid state with relatively shorter lifetimes, indicating the formation of a single species which is also substantiated through X-ray single crystal analysis. Latva's empirical rule[27] states that an optimal ligand-to-metal energy transfer process for $Ln^{III}$ needs ($\Delta E = T_{0-0} - {}^5D_J$) 2500−4000 $cm^{-1}$ for $Eu^{III}$ and 2500−4500 $cm^{-1}$ for $Tb^{III}$. The triplet energy level of the two salicylamide ligands is higher than the $^5D_0$ level of $Eu^{III}$ (17 250 $cm^{-1}$) and the $^5D_4$ level of $Tb^{III}$ (20 400 $cm^{-1}$). This, therefore, supports the observation of stronger sensitization of the terbium complexes than the europium complexes because of the smaller overlap between the ligand triplet and the europium ion excited states. On the other hand, a quenching mechanism through a low-lying charge transfer state because of the low reduction potential of the $Eu^{III}$ ion and the presence of the electron pairs of the aliphatic nitrogens may account for the relatively lower quantum yield and lifetime of $Eu^{III}$ complex than that of $Tb^{III}$.

(28) Horrocks, W. D., Jr.; Sudnick, D. R. *J. Am. Chem. Soc.* **1979**, *101*, 334.

## Conclusions

We presented here two novel structure-related tetrapodal ligands which can have different conformations and thus result in the formation of metal complexes with diverse structures using a new topological approach. It is noteworthy that subtle variation of the terminal group from benzene to pyridine of salicylamide terminal groups affects the coordination environment of the tetrapodal ligand which considerably changed the overall molecular structures from 3D frameworks to the dimer or 1D helical chains. To the best of our knowledge, compound **8** represents the first 1D helical chain obtained by linking salicylamide ligands with $Ln^{III}$ ions reported till now. The photophysical properties of the lanthanide complexes can also be fine-tuned by changing the terminal group of salicylamide which have significant influence on the coordination environment. These results serve to illustrate the potential of salicylamide ligands both with regard to constructing interesting supramolecular structures and for purposes of incorporating predictable physical properties. From a more general perspective, the coupling of polymer and luminescence in a material has interesting prospects for the development of luminescence materials.

**Acknowledgment.** The authors acknowledge support from the National Natural Science Foundation of China Research (Grants 20771048, 20431010, 20621091, and J0630962).

**Supporting Information Available:** CIF files, tables of interatomic distances and angles for compounds **1**−**8**, and figures with phosphorescence spectra of $Gd^{III}$ complex of ligand $L^I$ and $L^{II}$, and the room-temperature solid-state phosphorescence lifetime of Eu, Tb complex of ligand $L^I$ and $L^{II}$. This material is available free of charge via the Internet at http://pubs.acs.org.

IC8008267